Geothermal as resource for megacities

Carlos Vargas
Universidad Nacional de Colombia https://orcid.org/0000-0002-5027-9519
Luca Caracciolo (luca.caracciolo@fau.de)
Friedrich-Alexander Univerisity
Philip Ball
Friedrich-Alexander Univerisity

Article

Keywords: Megacities, people, energy

Posted Date: January 13th, 2021

DOI: https://doi.org/10.21203/rs.3.rs-138874/v1

Version of Record: A version of this preprint was published at Communications Earth & Environment on March 18th, 2022. See the published version at https://doi.org/10.1038/s43247-022-00386-w.

Abstract

33 Megacities are distributed around the world, a number that will increase to 43 by 2030. Megacities are critical for the world's economy, however, their management is particularly challenging in terms of transportation, water, waste, sanitation, security, electricity, and environmental impact. The increase of energy demand, in parallel to population growth and climate change, requires investment in sustainable energies. Geothermal energy – differently from solar, wind and hydroelectric is independent from weather conditions. A number of megacities around the world are located in areas with anomalous geothermal gradients, proximal to the margins of tectonic plates. This colocation makes geothermal an attractive resilient, baseload, low-carbon, energy source helping Megacities reduce their environmental impact. In this paper, we discuss the advantages of using geothermal energy, leading the study for the city of Bogotá, and applying the same workflow for Los Angeles and Jakarta. We aim to provoke the inclusion of geothermal in energy policies of other megacities around the world.

1. Introduction

The 2007 was the year when, for the first time in human history, the percentage of people living in cities exceeded that of people living in the country (Ritchie and Roser, 2020). Today, > 50% of world's population lives in urban areas, this is forecast to increase to 68% by 2050. Urban centres account for 67–76% of global final energy consumption of which an estimated 71–76% is fossil fuel derived (Seco et al. 2014). The associated greenhouse gas emissions (GHG) will grow from 70–80%, of the world's GHG discharges in 2050 (IEA, 2008). By 2050 the energy growth for heating and cooling of buildings could increase between 7–40% based on 2010 statistics (Güneralp et al., 2017). The Urban Heat Island (UHI), effects within mega-urban cities (EPA, 2020) will magnify the issues associated with global warming (Huang et al., 2019). Dealing with these challenges requires careful planning and optimisation of economic resources.

The increasing population in urban areas determined the escalation of megacities (city with a population of > 10 millions). There are 33 megacities around the world, a number that will rise to 43 by 2030 (Population Division of *United Nations*, 2018; Fig. 1). Notably, megacities today generate about 20% of the world's GDP. Megacities around the world face six common challenges: transportation, electricity, water, waste, sanitation, and security. It is therefore clear the importance of megacities, especially in light of environmental challenges and climate change at global scale.

Both energy demand and consumption will increase in parallel to population growth making electricity and the decarbonization of heating and cooling needs one of the most challenging issues to deal with for future of megacities. The majority of megacities are distributed in less developed regions which also those experiencing dramatic economic growth (Table 1). It is imperative therefore that sustainability and energy resilience is part of the development strategies for megacities. Despite the technological advancement, the use of sustainable, and greener forms of energy are undeveloped, (Hoornweg and Freire, 2013).

While renewable energies like wind and solar are accounted as potential suppliers for megacities, geothermal energy is rarely considered. In fact, a number of megacities around the world are located in regions with anomalous geothermal gradient, especially around the ring of fire (Fig. 1).

Geothermal energy for power production, today, can be applied using conventional, high and low temperature hydrothermal systems, Enhanced Geothermal Systems (EGS) and Advanced (closed loop) Geothermal Systems (AGS) (e.g. Ball, 2021a, b). In this paper we evaluate the use of geothermal energy and its potential contribution to the energy demand of megacities. We lead the study with Bogotá (Colombia), and follow the same workflow with Los Angeles (California) and Jakarta (Indonesia) as case studies. However, this concept could be easily applied to any other megacity of the world in the nearby of a geothermal anomaly.

1.1 Energy demand of megacities

Energy demand from megacities varies according to the level of development. In 2011, megacities in Northern America, Europe, and Japan used on average, per capita, more than 60 GJ (16.6 MWh) – and up to 100 GJ (27.7 MWh) e.g., Los Angeles and New York (Kennedy et al., 2015). Megacities in other parts of the world are quite often below 20 GJ (5.5 MWh), largely because two thirds of the megacities are in regions with warm climate (37% in the subtropics, 37% in the tropics, and 26% in the temperate zone; Table 2). In temperate climates, the demand of energy increases in cold months for heating. Most cities require cooling, with the energy for air conditioning being largely derived from electricity, hence depending on the available capacity of power generation and the existing grid

The implications of global warming combined with seasonal variations and the UHI effect may lead to power shortages if infrastructure/planning is not updated. The impact of the UHI alone reveals that temperatures today in cities can be an estimated 0.5-4 °C above unpopulated areas (EPA, 2020). Simple analysis presented in supplementary tables S1 and S2 suggest that the dominant impact of an average 1.5 °C and 3.0 °C temperature increase, is an increase in power use required for cooling, resulting in an estimated 14% and 22% increase in energy. Megacities in a global warming scenario could see a dramatic increase in cooling needs, which poses a problem regarding planning of new construction and retro-fitting. Future buildings may need to be constructed to keep the heat out, rather than in.

In addition to energy demands, climate change may be putting strain on the water supply. Megacities located in the subtropics might experience lower than average precipitation as weather patterns change. Water resources could be impacted requiring access to future water supplies from desalination or recycling of waste-water, all of which increases the future energy demand. At least 19 of the 30 megacities included in Table 1 obtain more than one third of the water supply from both surrounding areas and surface waters (Keys et al. 2018).

1.2 How can geothermal help megacities?

Advances in Conventional, EGS and AGS facilitate the concept of producing, low-carbon, sustainable, electricity adjacent to large population centres. In addition, low-grade heat may be used directly in district heating/cooling and in GSHP decarbonizing heating and cooling needs for individual houses or offices (Ball, 2021a, b). Furthermore, medium- and low-enthalpy geothermal energy can be used to decrease both operation costs and environmental impact from a broad range of industries including desalination of water, green houses, fish farming, brewing/fermenting, chemical products, automotive and large-scale production industry (Ball, 2021a). The combined approach of geothermal for heating and cooling and for electricity production therefore enables geothermal to decarbonize significant amounts of the energy needs especially if it is developed in conjunction with solar Photovoltaics (Solar-PV), wind power and improved insulation technologies for existing and new office building and homes.

2. Energy Demand And Consumption In Three Megacities

2.1 Colombia and Bogotá

With more than 75% of the population living in urban areas, Colombia is nowadays a highly urbanized country. Colombia's electric energy use per year is estimated to be 1,356 kWh per capita (WD, 2020). In 2018 Colombia had an installed energy capacity of approximately 17,312 MW, 63% of energy is derived from hydroelectric power, 29% from fossil fuels (gas and coal), the rest of the balance is from renewables (wind and solar) and other minor thermal sources (Fitch 2019).

Bogotá has grown to a population of ~ 10,700,000 within an area of ~ 397 km^2 (Table 1). The development of urban and industrial settlements benefit from a relatively flat topography within the broad plateau of the Eastern Cordillera of Colombia. Bogotá has a largely isothermal climate that typically varies from 7 °C to 19 °C, and receives the electricity provided by three biomass, two hydroelectric power and one gas/coal thermoelectric plant. The public transport sector is the highest consumer of energy derived mostly from petroleum products (gasoline and diesel) and subordinately from electricity. Both the industrial and residential sectors consume electricity and natural gas, while the sector for services requires electricity and petroleum products (Pardo Martinez, 2015). The energy consumption of Bogotá city in 2017 reached a total of 9241.5 GWh, representing the 17% of the total electricity of Colombia (UPME, 2018).

Droughts recently exposed Bogotá to an interruption of energy supply from its hydroelectric plants. The el Niño event in 2015–2016, caused significant drought leading to reductions in power output (Fitch 2019). According to statistics from 2018, energy demand in Colombia increased by 3.3%, reaching a total of 1159 kWh per capita (British Petroleum, 2019), and may grow 2.6% yearly, from 2019–2022 (UPME, 2018). Future growth is being met by an increase in gas, wind and solar projects, resulting in a net decrease in the share of power from hydrothermal plants (Fitch, 2019). In Colombia there are two geothermal projects currently planned for development, the 190 MW Macizo Volcánico del Ruiz and the 138 MW Tuviño geothermal power plant (Bullock, 2018).

2.2. California and Los Angeles

The United States of America are the second energy consumer in the world after China, and California - its most populous state - is the second in the country after Texas, in terms of total energy consumption (EIA 2020). The EIA ranks California as the world's fifth-largest economy which relies on numerous energy-intensive industries. California's population is highly urbanized with 97.8% of the population living in urban setting (RHI, 2020). California's installed electricity capacity is approximately 80,000 MW. In addition California imported 77,229 GWh of electricity in 2019 (Nyberg, 2020). California's residential use, is one of the lowest per capita, in the USA, at 6,684 kWh, compared to an average of 11,888 kWh (EIA, 2009). California's total energy consumption, per capita, is 202 million Btu, again one of the lowest in the USA, in part to its favourable climate (EIA 2020). The Californian energy mix in-state is dominated by natural gas (42.97%), large hydro (16.53%) and nuclear (8.06%). Renewables make up the 32.09% of the energy mix, and is dominated by solar (14.22%), wind (6.82%) and geothermal (5.46%), (Nyberg 2020). In 2019 geothermal energy produced 5.46% of California's in-state generation portfolio (Nyberg 2020). The geothermal installed in California accounts for 91% of the USA's steam-powered capacity, since 2000, however, nearly 90% of the new capacity added uses binary-cycle capacity (Linga, 2020). Importantly in California, since 2016, closed-loop binary geothermal developments have been designated as zero carbon (CARB, 2016).

Los Angeles (LA) metropolitan area has grown to a population of 12,458,000 within an area of ~ 12,562 km^2 (Table 1). The city of LA is a coastal city, built over a deformed, ~ 9 km deep, sedimentary basin with significant oil and gas resources (Bilodeau et al. 2007). Climatically the latitude and geographic location and proximity of coastal mountains give LA a temperate Mediterranean climate. There are no geothermal power plants located within Los Angeles County. Integrated energy systems support LA's energy needs, via an extensive transmission and distribution infrastructure (LADWP, 2017). In 2020, the cities energy mix was derived from 34.1% renewable power, including 8.9% from geothermal resources, 21% coal, 4,1% hydroelectric, 27.2% natural gas, 12.5% from nuclear (LADWP, 2020). In 2019, according to the California Energy Commission, the energy consumption of LA reached 66,118.6 GWh, which corresponds to 46,556.1 GWh non-residential, and 19,562.5 GWh in the residential sector (CEC, 2020). The average LA resident uses about 5,900 kilowatt-hours of electricity per year (LADWP, 2020). Both commuting time and distance to reach the workplace means that the transport sector uses 49% of California end-use energy consumption (EIA, 2017). On the other hand, the industry requires 24.5% of state energy use and represents the second-largest energy consumer. Commercial 12.5%, and residential end-use reaches 14% of total energy consumption (EIA, 2020).

California has one of the most decarbonized energy systems in the USA, as a result of proactive renewable energy policies. Yet, climate impacts such as drought and forest fires have highlighted some of the limitations of an energy system that is reliant on intermittent sources such as wind and solar PV. There are several high-profile rolling-blackout events in California, highlighting the lack of resilience within the state impacting solar, wind and hydrothermal resources (Clemente, 2016). The LADPW 2017 roadmap for LA's energy resource is strongly aimed at decarbonizing its emissions, and as coal is phased out geothermal, wind and solar are targeted to play a significant role.

2.3. Indonesia and Jakarta

Indonesia is the most populous country in Southeast Asia and the fourth most populous country in the world. According to IEA (2020), its domestic energy consumption is large, fast-growing, and inefficient due to an inadequate infrastructure and a disperse territory which extend on more than 17,000 islands. Despite signing the 2015 Paris Agreement, Indonesia is, currently, well off-target to meet the reduction in greenhouse gas emissions (IEA, 2020). Indonesia is a producer of old-style biomass and waste-burn energy for its residential sector, particularly in the distant areas not connected to the country energy grid. The country is using fossil fuels to expand its industrial capabilities and develop its electricity and transportation sectors. Presently, the generation capacity in Indonesia is lower than the demand for electricity, leading to frequent power shortages (Christina, 2019). Indonesia has an estimated 71 GW of installed capacity (IDNF, 2020), however, increased urbanization is contributing to an annual 8–9% increase in energy demand, which is not being met despite 15% of Indonesians not having access to the electric grid (Heggie, 2015). As the country modernises, the per-capita electricity consumption is growing rapidly from 0.2 MWh/capita in 1990 to 1.0 MWh/capita in 2018 (IEA, 2020).

Indonesia is the world's second-largest producer of geothermal energy, with 2,130.7 MW of installed power generation capacity from 16 Geothermal Power Plants. By 2030 the country aims to grow capacity to 8,007.6 MW (Richter, 2020). This still only represents a fraction of the estimated 29 GW of geothermal potential within the country (ADB and WB, 2015). In 2019 the Indonesian energy mix for electricity production was coal 59%, natural gas 20.8%, oil 4.1%, hydroelectric 7.1%, geothermal 4.7%, biofuels 3.6% with wind, solar and waste heat making up the remaining 0.7% (IEA, 2020). Total energy consumption use in Indonesia is dominated by the transport sector, 34%, followed by industry, 34.8% and residential end use 22% (IEA 2020). The rapid growth in the transport sector could be due to the dramatic increase in the number of private vehicles, due to expanding mobility in the middle-class (Deendarlianto et al. 2017).

Today, Jakarta, is reported to have a population of 10,517,000 within an area of 556 km^2 (Table 1). Jakarta is a lowland area, built on an alluvial plain, with a relatively flat topography. Jakarta is characterized by a tropical monsoonal climate with a mean temperature variation between 24 °C and 29.5 °C. Jakarta is the most vulnerable region in SE Asia to the impacts of climate change and is vulnerable to floods, landslides, droughts, and sea level rise (Yusuf & Francisco, 2009). Decarbonizing the economy, through renewables energy growth, is critical for Jakarta and Indonesia to develop to energy sovereignty and self-sufficiency, as the country drives for modernization and access to electricity for its people (IEA, 2020).

3. Geodynamic And Geothermal Setting

3.1. Geothermal system near to Bogota

Bogota is built on a sedimentary succession spanning from marine Mesozoic, continental Cenozoic sedimentary rocks, Plio-Quaternary glacial and fluvial deposits filling a late Triassic rift system formed

during the break-up of the super continent Pangea (Pindell, 1985). The late Miocene inversion of this basin relates to the exhumation of the Eastern Cordillera that followed the collision of the Panama Arc and more generally to the convergence of the Nazca and Caribbean plates under the South American continent (Pennington, 1981).This process triggered the emplacement of foothill fault systems with trend SSW-NNE, and a long lithospheric fracture - the Caldas Tear - connected to an extinct rift (12 – 9 Ma) namely the Sandra Ridge (Figs. 2 and 3; Londsdale, 2005;) with a trend almost W-E. The kinematics of this fracture is currently evidenced by the presence of a 240 km offset between the subduction seismicity and volcanism (Fig. 3a). Barrera et al. (2018) proposed that the lithospheric tear represents a mechanism for the emplacement of thermal anomalies related to late Miocene to Pliocene magmatic intrusions in the central sector of the Eastern Cordillera basin (Fig. 3b) (Siravo et al., 2018). The numerical modelling by Siravo et al. (2019) suggests that the flattening of the Nazca or Caribbean plates in this area occurred between 10 – 6 Ma may explain the topography of the Eastern Cordillera and the thermal behaviour of the upper crust, probably as consequence of a highly hydrated asthenospheric wedge. Thermal anomalies north of Bogotá have been identified through (a) geothermal gradient data from exploratory wells (Vargas et al., 2009); (b) range of maturation of coal (Pedraza-Fracica and Mariño, 2016); (c) remaining hydrothermal activity in the extinct volcanoes to the north of Bogota (Pardo et al., 2005), and (d) numerous faults and fractures that control hot springs in the region (Gómez et al., 2015). The geothermal gradients of these anomalies reach locally 70 °C/km (Vargas et al., 2009) and could be linked to regional delamination processes and/or the flow of hydrothermal fluids through the sedimentary sequence of the Eastern Cordillera basin (e.g. Monsalve et al., 2019). Viera and Hamza (2014) estimated the geothermal resource base (GRB) in Colombia to have a mean value of 294 GJ/m^2, while the recoverable part is appraised to be 31 GJ/m^2.

3.2 Geothermal system near to Los Angeles

The southern region of California, and the continental borderlands, records a complex geological history that involves notable tectonic features like the Los Angeles Basin (LAB), the Peninsular Ranges (PR), and the California Transverse Ranges (TR). The LAB is an early Miocene pull-apart basin located on the edge of the Pacific Plate, and bounded by the TR and PR, promoting a contrasting structural relief (Fig. 5). The basin forms as part of a distributed transform system, which represents the switch from subduction to a transform-related margin at ~ 8 Ma as subduction diminished (Atwater and Stock 1998). The basement rocks in this region are Mesozoic orogenic, meta-igneous, rocks (Humphreys and Coblentz, 2007). There are several large-scale strike-slip faults within the basin, such as the Newport-Inglewood (NIFZ) and the San Andreas Fault (SAFZ). The regional principal stress field, in the LAB is orientated north-south indicating the major faults in the basin are, presently, undergoing transpressional deformation (Lund Snee and Zoback, 2020). Tomographic images indicate that the lithosphere is thinned to 40–50 km, in the LAB region, whereas the lithospheric thickness is greater 70–80 km, in the PR and TR regions, (Lekic et al., 2011). Significant crustal thinning is observed in the LAB where Moho depths are reported to be as shallowing from 25 to 12 km (Clayton, 2020).

Extension was accompanied by significant volcanism in the middle-Miocene along the outer

edge of the Inner Borderland (Legg et al., 2004). Recent hydrothermal activity evidences are observed present-day along the TR and PR (Luedke and Smith, 1981). Measurements of $^{3}He/^{4}He$ ratio in the Los Angeles Basin suggest that there is a strong mantle contribution of helium from long-lived large strike-slip fault systems which intersect with the mantle (Boles et al., 2015). Present day surface heatflow within the LAB is variable ranging from 63 to 85 mW/m^2. The variation has been proposed to be related to the combined effects of sedimentation, local structural complexities, or reflecting non-steady-state conditions related to magmatism and/or hydrothermal circulation (Zuza and Cao, 2020).

3.3 Geothermal system near to Jakarta

Java is a volcanic island arc in the Indonesian archipelago at the southern margin of the Eurasian plate. Inland, several tectonic features as the Lembang Fault (LF), Kendeng Fault (KF), and Cimandiri Fault (CF), define the volcanic arc (Fig. 6). This converging margin forms where the Indo-Australian plate (IAP) is subducting under the Eurasian plate (EAP). Subduction has been continuous throughout the Cenozoic, in the segment that forms the island of Java the subduction is observed to be orthogonal (Clements et al., 2009). Structural inheritance from Cretaceous extension related to the formation of the volcanic arc complicate the structural setting (Clements et al., 2009). Following the onset of the arc, thrusting and deformation, of the arc, is considered to have started during the Middle Eocene (Clements et al. 2009). Thrusting of the arc has displaced arc volcanics northwards by more than 50 km in western Java, eliminating the Paleocene arc-related flexural basin (Clements et al., 2009). Jakarta is located north of the Barbaris thrust which forms the northern limit of Neogene thrusting (Clements et al. 2009). Beneath the Paleogene, Neogene and recent sediments of the Sunda shelf basins the basement of Jakarta is the Mesozoic Sunderland continental crust.

West Java has the highest density of volcanics (Setijadji, 2010). The youngest episode of volcanic activity resumed in the Late Miocene producing a younger arc to the north of the older arc, and volcanism continues to the present day (Cottam et al., 2010). Seismic tomography reveals the mantle in west Java is characterized by low vP anomalies, low vS anomalies and high vP/vS ratios, which is indicative of a high fluid content, due to partial melting, originating from the subducted slab (Rosalia et al., 2019). This tectonic setting promotes geothermal anomalies (with abundant spring-waters) associated to volcanic provinces throughout the island of Java. Heatflow models reveal that onshore basins of Northwest Java have considerably high values with an average of 94.05 ± 26.42 mW/m^2 (Putra et al., 2017). While heat flow varies in the basin, even in the absence of hot-springs, anomalously high heatflows may be due to processes of heat refraction or heat transfer by groundwater flow regimes (Putra et al. 2017).

4. Methodology

The concept of GRB refers to the thermal energy Q stored in a volume V of rock in the subsurface and is usually estimated by means of the volumetric heat in place (VHIP) approach proposed by Muffler and Cataldi (1978). It depends on both thermal rock properties and the distribution of the geothermal gradient. Although this approach provides a simplified general idea of the thermal energy on large scales, large

uncertainties remain due to the variability of the medium of variables such as density ρ, porosity Φ, heat capacity *C*, and temperature contrast (ΔT) in the region of interest. This method is based on Eq. (1), where the subscript *r* refers to rock and *w* to water:

$$Q = [(1 - \Phi) * \rho_r * C_r + \Phi * C_w * \rho_w] V * \Delta T \quad (1)$$

However, determining the potential geothermal power is difficult due to the scarcity of available information, furthermore uncertainties relating to newer AGS techniques and their efficiency at mining heat vs. utilizing hydrothermal waters to extract heat is still open for debate, since commercial developments are still not commonplace. Therefore assessment of a pure-play thermal resource is not included in this analysis.

In the Eastern Cordillera the GRB assessment therefore is based on estimates from O&G wells, and associated spring-waters, we assume a regional play with geothermal gradients between 30–40 °C/km (Fig. 3). Using the EMAG2 database (Maus et al., 2009), Li et al. (2017) estimated the Curie Point depths (CPDs) for this area ranging between 30–40 km. Nevertheless, the most surficial CPDs match with the area of the largest density of spring waters (LDSW) in the Eastern Cordillera. To compensate the limitations in resolution of the EMAG2, we integrate it with the local magnetic database reported in Briceño et al. (2008) to improve the resolution and geometry of anomalies (Fig. 4) and assure trends in the interpolation process. Estimations of the CPDs reported in this work follow the approach proposed by Bouligand et al. (2009) and use the code Pycurious (Mather and Delhaye, 2019). Details of the method and parameters used are provided in the *online data repository*. Figure 4 shows the results of the estimation of the CDPs and highlight a surficial indenter of CPDs (< 30 km) coming from the west and located in the middle of the LDSW area. This anomaly may be responsible of the heating of the water springs dislocated along the fault system in the crest of the Eastern Cordillera with trend NNE and their complex intersections.

The same principle that was applied to the Eastern Cordillera and Bogata, was used for the cities of Los Angeles and Jakarta. We simplify the model and hypothesize that - even considering the discrepancy between CPDs estimations - the role of the tectonic features controlling the spring-waters and the area encompassing them are fundamental to define the volume of potential reservoir that is storing the thermal energy. Therefore, we assume the elliptical envelope that encompasses the LDSW as the best alternative for a better constraining of the area. While the areas, depth, and thickness of recoverable resources have been assumed according to the regional geology of the three areas, an average porosity of 5%, fluid heat capacity of 4000 J/kg ºC, rock heat capacity of 850 J/kg ºC, specific heat capacity of 920 J/kg °K, and an efficiency as low as 0.1% have been set as general values for the three areas.

5. Results

Table 3 summarizes the main volumetric parameters used for estimating the potential geothermal energy, following the method of Muffler and Cataldi (1978), and Viera and Hamza (2014). In addition based on

the regional population statistics compiled in Table 1, and statistics reported in Sect. 2, are used to estimate the power consumed by all inhabitants for these megacities and their metropolitan areas. The results are presented below for each megacity studied:

5.1. Bogotá

For Bogata, we estimated the maximum value of recoverable resource within an area of ca. 7500 km^2. We assumed an average depth of 3 km, a 30 m thick sandstone reservoir (the Eastern Cordillera Basin that is approximately 11 km thick, and hosts at least one regional reservoir unit, the Une Formation; Barrero et al., 2007). Our estimations suggest a rough value of resource of approx. 16,603.1 GWh, corresponding to ~ 1.14 times the energy per capital consumed by all people located in the metropolitan area, as per Table 3. That means a potential coverage of the total residential demand with this resource. This estimated amount of energy may guarantee enough baseload residential electric resources, solely through the use of geothermal derived electricity. .

5.1.1. Los Angeles

Within the region of Los Angeles, spring-water occurrences cover an area of approx. 9.400 km^2. Where the CPDs are relatively surficial, coincides with an area ranging between 15–25 km. As with Bogata, we followed same approach to estimate the maximum recoverable resource, using formula (1). Thereby assuming an average depth of 3 km, one 450 m thick reservoir (half of the thickness than in NW Geysers Geothermal Field area, Antúnez et al., 1994). Our estimations suggest a resource of approx. 312,138.8 GWh, corresponding to approx. 3.75 times the energy per capita consumed by all inhabitants that live in this megacity based on the assumptions made in Table 3.

5.1.2. Jakarta

In the region of Jakarta, the CPDs are reported to be < 25 km deep. The distribution of volcanic cones and spring-water occurrences were taken as criteria for defining the main area for focusing a detailed geothermal exploration near to Jakarta city. The ellipse envelope that encompasses these features defines an area of approx. 9.100 km^2. Using same approach as in previous cases, we assume an average depth of 1.0 km, one 30 m thick reservoir (using similar thickness from the Wayang Windu geothermal field, West Java, Bogie et al., 2008). The estimations indicate a resource of approx. 20,145.1 GWh, corresponding to 1.92 times the energy per capita consumed by all people that are currently living in this megacity.

6. Environmental Impacts And Resource Administration

The estimates presented here only represent that for conventional and EGS-types of geothermal exploitation. These estimates already highlight that geothermal derived power can be sufficient to decarbonize the present energy needs. In some cases it may also help support and decarbonize the future energy needs resulting from climate change and global warming (Supplementary tables S1 and S2).

Importantly, geothermal derived power is not as vulnerable to environmental changes, and, importantly, it provides a low-carbon baseload power.

Advances in geothermal completions utilizing binary, closed-loop or AGS, fully mitigate these environmental issues common with flash-geothermal power plants (Bravi and Basosi, 2014; CARB, 2016; Ball 2021a). While binary, closed-loop developments or AGS can increase the cost level of geothermal development, these newer concepts allow a wider deployment of geothermal energy, for power production and provide long-term cost-efficiencies to regions which prioritise GHG reduction targets (Ball 2021a, b). Geothermal is a baseload technology which meets significant energy resilience needs which wind and solar cannot deliver as intermittent sources. Geothermal power could therefore lead to the closure of coal and gas power (Ball 2021a, b), whereas the preference of the apparently cheaper wind and solar-PV technologies, effectively lock a economies into a carbon based gas or coal infrastructure (Gillingham and Huang, 2018).

Promotion of geothermal systems is sometimes challenged due to the initial high installation costs compared with other energy resources. Although it should be remembered that geothermal offers a baseload power whereas wind and solar-PV are intermittent sources that induce additional costs for storage (e.g. battery) and these intermittent sources also bring instability to the grid, requiring that baseload power-stations (for example gas or coal) be maintained on standby to ramp up and down to meet the gaps in energy supply (Ball 2021b). In future geothermal could also provide this flexibility providing dispatchable power as geothermal power plants are developed. With greater geothermal development, stakeholder management is critical, at public, regional and governmental levels. This is particularly true for the development of enhanced geothermal systems (EGS). Poor communication and education within local communities regarding the value of regional and local energy resources, potential hazards and their mitigation or management, could lead to backlash and even social rejection. If managed properly, the geothermal resource could provide significant decarbonization of the power needs for megacities. In addition, geothermal can bring local benefits (e.g. job creation) and reduce the public expense in the energy sector. GEOENVI (2020) recently reported that geothermal has brought an annual saving of 2.6% of GDP to the Icelandic economy.

Geothermal power is both a baseload source and flexible, thus providing the perfect partner with wind and solar-PV and hydroelectric resources. Given the geotectonic position of the world's megacities, we see a huge potential for the use of geothermal power which would also reduce the environmental impact and help contrasting the energy challenge in overpopulated areas. It should be noted that lower grade solutions utilizing direct use technologies such as Ground Source Heat Pumps (GSHP) and district energy systems, provide additional baseload decarbonization of heating and cooling needs. Such technologies, if retrofitted into existing building stock and implemented in new buildings, reduce the primary electric demand (Ball et al. 2021a, b). Finally, if all geothermal solutions are investigated, including the direct use of geothermal district heating and GSHP's, then additional benefits of a low-carbon energy system may be found, raising the quality of life for many people and helping to reduce energy poverty.

7. Conclusions

The use of geothermal energy near to megacities located along the margins of tectonic plates may guarantee a sustainable and resilient form of energy to supply decarbonizing residential, industry, transportation and other needs. Critical to the uptake of geothermal energy, however, is a positive government action that may include a carbon tax, investment into research and development of geothermal resources and the establishment of policies or tax-breaks that encourage the exploration and development of geothermal resources.

References

1. ADB and WB, (2015). Unlocking Indonesia's geothermal potential, Asian Development Bank and The World Bank, https://openaccess.adb.org; https://openknowledge.worldbank.org.
2. Amante, C. and Eakins, B.W., (2009). ETOPO1 1 Arc-Minute Global Relief Model: Procedures, Data Sources and Analysis. NOAA Technical Memorandum NESDIS NGDC-24. National Geophysical Data Center, NOAA. doi:10.7289/V5C8276M [Data accessed on May 17, 2020].
3. Antúnez, E.U., Bodvarsson, G.S., and Walters, M.A., (1994). Numerical simulation study of the Northwest Geysers Geothermal Field, a case study of the Coldwater Creek Steamfield. Geothermics, 23(2): 127-141.
4. Atwater, T., and Stock, J. M., (1998), Pacific-North America plate tectonics of the Neogene southwestern United States: An update, Int. Geol. Rev., 40, 375–402.
5. Ball, P.J., (2021a). A review of geothermal technologies and their role in reducing greenhouse gas emission. ASME Journal of Energy Resources Technology, 143. https://doi.org/10.1115/1.4048187
6. Ball, P.J., (2021b). Macro energy trends and the future of geothermal within the low-carbon energy portfolio ASME Journal of Energy Resources Technology, 143, https://doi.org/10.1115/1.4048520
7. Barrero, D., Pardo, A., Vargas, C.A., Martínez, J.F., (2007). Colombian sedimentary basins: Nomenclature, boundaries and petroleum geology, a new proposal. Agencia Nacional de Hidrocarburos. p. 92. ISBN: 978-958-98237-0-5
8. Barrera, C. A., Vargas, C.A., and Cortes, J.E., (2018). Establishing geothermometric constraints on the local geothermal gradients: Case study of the Eastern Cordillera Basin, Colombia. Geodesy and Geodynamics, 9, (4), pp. 271-280, ISSN 1674-9847, https://doi.org/10.1016/j.geog.2017.08.004.
9. Bilodeau, W. L., Bilodeau, S. W., Gath, E.M., Oborne, M., and Proctor, R.J., (2007). Geology of Los Angeles, California, United States of America. The Geological Society of America, 13 (2), pp. 99-160 .
10. Bogie, I., Kusumah, Y.I. and Wisnandary, M.C., (2008). Overview of the Wayang Windu geothermal field, West Java, Indonesia. Geothermics 37: pp. 347–365.
11. Boles, J. R., Garven, G. Camacho, H. and Lupton, J. E. , (2015), Mantle helium along the Newport-Inglewood fault zone, Los Angeles basin, California: A leaking paleo-subduction zone, Geochem. Geophys. Geosyst., 16, pp. 2364–2381, doi:10.1002/2015GC005951.

12. Bouligand, C., Glen, J. M. G., and Blakely, R. J., (2009). Mapping Curie temperature depth in the western United States with a fractal model for crustal magnetization. Journal of Geophysical Research, 114(B11104), 1–25. https://doi.org/10.1029/2009JB006494
13. Bravi, M. and Basosi, R., (2014). Environmental impact of electricity from selected geothermal power plants in Italy. Journal of Cleaner Production, 66: 301-308. http://dx.doi.org/10.1016/j.jclepro.2013.11.015.
14. Briceño, L.A., Rey, Vargas, C., Hernandez, C.A., Zamora, O., (2008). A. New Magnetic Anomalies Map of Colombia MAM. Earth Sciences Research Journal. v.12, Spec. Ed., p.7 - 12.
15. British Petroleum, (2019). BP Statistical Review of World Energy, online resource.
16. Bullock, E., (2019). Geothermal Country Overview: Colombia. GeoEnergy Marketing Services, Online resource, accessed on the 11/28/2020,
17. CARB, (2016). California's 2000-2014 Greenhouse Gas Emission Inventory, Technical Support Document. California Environmental Protection Agency, Air Resources Board, Air Quality Planning and Science Division, pp.174.
18. CEC, (2020). Electricity Consumption by County, California Energy Commission. Online resource, accessed 12/22/2020
19. Christina, B., (2019). Indonesia president criticises state power company over blackouts. Reuters, Online resource accessed, on the 11/30/2020.
20. Clayton, R., (2020). A Detailed Image of the Continent-Borderland Transition Beneath Long Beach, California, Geophys. J. Int. 222, 2102–2107, doi: 10.1093/gji/ggaa286
21. Clemente, J., (2016). California's Growing Imported Electricity Problem. Forbes.
22. Clements, B., Hall, R., Smyth H.R., and Cottam, M.A., (2009). Thrusting of a volcanic arc: a new structural model for Java, Petroleum Geoscience, 15, pp. 159–174, DOI 10.1144/1354-079309-831
23. Deendarlianto, Widyaparaga, A., Sopha, B.M., Budiman, A., Muthohar, I., Setiawan, I.C., Lindasista, A., Soemardjito, J., and Oka, K., (2017). Scenarios analysis of energy mix for road transportation sector in Indonesia. Renewable and Sustainable Energy Reviews, 70, 13-23, https://doi.org/10.1016/j.rser.2016.11.206
24. EAI, (2009) Household Energy Use in California: A closer look at residential energy consumption. Online resource.
25. EIA, (2017). State Energy Data System, Table C1, Energy Consumption Overview: Estimates by Energy Source and End-Use Sector.
26. EIA, (2020). California Profile. https://www.eia.gov/state/analysis.php?sid=CA#17. Consulted on May 19, 2020.
27. EPA, (2020). Heat Island Effect. United States, Environmental Protection Agency. Washington, DC. Online resource, accessed on the 11/26/2020
28. Fitch, (2019). Latin American Power Overview: Outlook, Financial Performance, Regulatory Risk and Investments. Fitch Group, London, UK, pp137.

29. GEOENVI, (2020). The many economic benefits Iceland got from using geothermal energy. GEOENVI. Online resource, accessed 12/13/2020.
30. Gillingham, K., and Huang, P., (2018). Is Abundant Natural Gas a Bridge to a Low-Carbon Future or a Dead-End? Energy Journal, 40 (2), pp. 1–26.
31. Gómez, J., Nivia, Á, Montes, N.E., Almanza, M.F., Alcárcel, F.A. & Madrid, C.A., (2015). Notas explicativas: Mapa Geológico de Colombia. En: Gómez, J. & Almanza, M.F. (Editores), Compilando la geología de Colombia: Una visión a 2015. Servicio Geológico Colombiano, Publicaciones Geológicas Especiales 33, p. 9–33. Bogotá.
32. Güneralp, B., Zhou, Y., Ürge-Vorsatz, D., Gupta, M,. Yu,S., Patel, P.L., Fragkias, M., Li, X, and Setog, K.C., (2017). Global scenarios of urban density and its impacts on building energy use through 2050. PNAS, 114 (34) p. 8945-8950; https://doi.org/10.1073/pnas.1606035114
33. Hoornweg, D.; Freire, M., (2013). Building Sustainability in an Urbanizing World. A partnership report.
34. Huang, K., Li, X., Liu, X., and Seto, K.C., (2019). Projecting global urban land expansion and heat island intensification through 2050. Environmental Research Letters, 14.
35. Humphreys, E. D., and Coblentz, D.D., (2007). North American dynamics and western U.S. tectonics, Rev. Geophys., 45, RG3001, doi:10.1029/2005RG000181
36. Nyberg, M., (2020). 2019 Total System Electric Generation. California Energy Commission, online. Resource accessed, 11/30/2020.
37. IEA, (2008). World energy outlook. Paris: International Energy Agency.
38. IEA, (2020). Countries: Indonesia.
39. IDNF, (2020). The total installed capacity of power plants in Indonesia reaches 71 GW, IDN Financials, online resource, accessed 12/01/2020.
40. Kennedy, C., Stewart, I., Facchini, A., Cersosimo, I., Mele, R., Chen, B., Uda, M., Kansal, A., Chiu, A., Kim, K., Dubeux, C., La Rovere, E.L., Cunha, B., Pincetl, S., Keirstead, J., Barles, S., Pusaka, S., Gunawan, J., Adegbile, M., Nazariha, M., Hoque, S., Marcotullio, P.J., González Otharán, F., Genena, T., Ibrahim, N., Farooqui, R., Cervantes, G., and Duran Sahin, A. (2015). Energy and material flows of megacities. PNAS, 112 (19): 5985–5990, www.pnas.org/cgi/doi/10.1073/pnas.1504315112.
41. Keys, P.W., Wang-Erlandsson, L., and Gordon, L.J., (2018). Megacity precipitationsheds reveal tele-connected water security challenges. PloS ONE, 13(3), e0194311. https://doi.org/10.1371/journal.pone.0194311.
42. LADWP, (2020). Los Angeles Department of Water and Power (LADWP). Online Resource, accessed on the 11/30/2020.
43. LADWP, (2017) Los Angeles Department of Water and Power 2017 Power Strategic Long-Term Resource Plan. Online resource, Los Angeles Department of Water and Power (LADWP), pp. 578.
44. Lekic, V., French, S.W., and Fischer, K.M., (2011). Lithospheric Thinning Beneath Rifted Regions of Southern California. Science 334, 783, DOI: 10.1126/science.1208898.

45. Li, C., Lu, Y. & Wang, J., (2017). A global reference model of Curie-point depths based on EMAG2. Sci Rep 7, 45129. Online resource.
46. Linga, V., (2020). Most U.S. Utility-Scale Geothermal Power Plants Built Since 2000 Are Binary-Cycle Plants, U.S. Energy Information Administration; Accessed November 8, 2020.
47. Luedke, R.G., Smith R.L., 1981. Map showing distribution, composition, and age of late Cenozoic volcanic centers in California and Nevada. U S Geol Surv Map, I-1091-C.
48. Lund Snee, J.E., and Zoback, M.D., (2020). Multiscale variations of the crustal stress field throughout North America, Nature Communications 11:1951, https://doi.org/10.1038/s41467-020-15841-5
49. Maus, S., Barckhausen, U., Berkenbosch, H., Bournas, N., Brozena, J., Childers, V., Dostaler, F., Fairhead, J. D., Finn, C., von Frese, R. R. B., Gaina, C., Golynsky, S., Kucks, R., Lühr, H., Milligan, P., Mogren, S., Müller, R.D., Olesen, O., Pilkington, M., Saltus, R. Schreckenberger, B., Thébault, E., Caratori Tontini, F. (2009). EMAG2: A 2 –arc min resolution Earth Magnetic Anomaly Grid compiled from satellite, airborne, and marine magnetic measurements, Geochem. Geophys. Geosyst., 10, Q08005, doi:10.1029/2009GC002471.
50. Mather, B. and Delhaye, R., (2019). PyCurious: A Python module for computing the Curie depth from the magnetic anomaly. Journal of Open Source Software, 4(39), 1544, https://doi.org/10.21105/joss.01544.
51. Monsalve, G., Jaramillo, J. S., Cardona, A., Schulte-Pelkum, V., Posada, G., Valencia, V., & Poveda, E., (2019). Deep crustal faults, shear zones and magmatism in the Eastern Cordillera of Colombia: Growth of a plateau from teleseismic receiver function and geochemical Mio-Pliocene volcanism constraints. Journal of Geophysical Research: Solid Earth. doi:10.1029/2019jb017835.
52. Muffler, P. and Cataldi, R., (1978). Methods for regional assessment of geothermal resources. Geothermics, 7(2-4), pp.53–89.
53. Pardo Martínez, C.I., (2015). Energy and sustainable development in cities: A case study of Bogota, Energy, DOI: 10.1016/j.energy.2015.02.003
54. Pedraza-Fracica, S. and Mariño, J., (2016). Thermal evaluation of 6 wells of the central part of the eastern cordillera (Colombia), from paleogeotherms: implications on thermal history and hydrocarbons. Ingeniería y Competitividad, 18 (1): 9 – 21.
55. Pennington, W. D., (1981). Subduction of the Eastern Panama Basin and seismotectonics of northwestern South America. Journal of Geophysical Research: Solid Earth, 86(B11), 10753–10770. doi:10.1029/jb086ib11p10753.
56. Pindell, J.L., 1985. Alleghenian reconstruction and subsequent evolution of the Gulf of Mexico, Bahamas, and Proto-Caribbean. Tectonics 4, 1–39.
57. Richter, A., (2020). Indonesia remains focused on becoming world top ranking geothermal country. Online resource, accessed 11/30/2020,
58. Rosalia, S., Widiyantoro, S., Nugraha, A.D., and Supendi, P., (2019). Double-difference tomography of P- and S-wave velocity structure beneath the western part of Java, Indonesia. Earthquake Science, 32: 12–25, doi: 10.29382/eqs-2019-0012-2.

59. Putra, S.D.H., Suryantini, and Srigutomo, W., (2016). Thermal modeling and heat flow density interpretation of the onshore Northwest Java Basin, Indonesia. Geotherm Energy, 4, 12, DOI 10.1186/s40517-016-0052-x
60. Salazar, S., Muñoz, Y., and Ospino, A., (2017). Analysis of Geothermal Energy as an Alternative Source for Electricity in Colombia. In: Geothermal Energy 5 (1), S. 27. DOI: 10.1186/s40517-017-0084-x.
61. Siravo, G., Faccenna, C., Gérault, M., Becker, T. W., Fellin, M. G., Herman, F., & Molin, P., (2019). Slab flattening and the rise of the Eastern Cordillera, Colombia. Earth and Planetary Science Letters, 512, 100–110. https://doi.org/10.1016/j.epsl.2019.02.002.
62. Siravo, G., Fellin, M. G., Faccenna, C., Bayona, G., Lucci, F., Molin, P., & Maden, C., (2018). Constraints on the Cenozoic deformation of the Northern Eastern Cordillera, Colombia. Tectonics, 37, 4311–4337. https://doi.org/10.1029/2018TC005162.
63. UPME, (2018). Boletin Estadísitico de Minas y Energía 2018. Report in Spanish.
64. Vargas, C.., and Mann, P., (2013). Tearing and Breaking Off of subducted slabs as the result of collision of the Panama Arc-Indenter with Northwestern South America. Bulletin of the Seismological Society of America, 103 (3): 2025-2046.
65. Vargas, C. A., Alfaro, C., Briceño, L. A., Alvarado, I., and Quintero, W., (2009). Mapa Geotérmico de Colombia, 2009. In proceedings of the X Bolivarian Symposium on Petroleum Exploration in Sub-Andean Basins, Colombia.
66. Viera, F.P., and Hamza, V.M., (2014). Advances in Assessment of Geothermal Resources of South America, Natural Resources, 05 (14), 897-913, DOI: 10.4236/nr.2014.514077
67. WD, (2020). Energy consumption in Colombia, World Data, online resource accessed 11/28/2020, https://www.worlddata.info/america/colombia/energy-consumption.php
68. Williams, C.F., Reed, M.J., Mariner, R.H., DeAngelo, J., and Galanis, Jr.S.P., (2008). Assessment of Moderate- and High-Temperature Geothermal Resources of the United States, USGS, Factsheet 2008-3082. https://pubs.usgs.gov/fs/2008/3082/pdf/fs2008-3082.pdf
69. Wright, T. L. (1991), Structural geology and tectonic evolution of the Los Angeles basin, in Active Margin Basins, AAPG Mem.
70. , vol. 52, edited
71. by K. T. Biddle, pp. 35–134, Amer. Assoc. Petrol. Geol., Tulsa, Okla
72. Wright, T. L. (1991), Structural geology and tectonic evolution of the Los Angeles basin, in Active Margin Basins, AAPG Mem.
73. , vol. 52, edited
74. by K. T. Biddle, pp. 35–134, Amer. Assoc. Petrol. Geol., Tulsa, Okla
75. Wright, T. L. (1991), Structural geology and tectonic evolution of the Los Angeles basin, in Active Margin Basins, AAPG Mem.
76. , vol. 52, edited

77. by K. T. Biddle, pp. 35–134, Amer. Assoc. Petrol. Geol., Tulsa, Okla
78. Wright, T. L. (1991), Structural geology and tectonic evolution of the Los Angeles basin, in Active Margin Basins, AAPG Mem.
79. , vol. 52, edited
80. by K. T. Biddle, pp. 35–134, Amer. Assoc. Petrol. Geol., Tulsa, Okla.
81. Yusuf, A.A. & Francisco, H., (2009). Climate Change Vulnerability Mapping for Southeast Asia Vulnerability Mapping for Southeast Asia. IDRC Canada.
82. Zuza, A. V., and Cao, W., (2020). Seismogenic thickness of California: Implications for thermal structure and seismic hazard, Tectonophysics, 782-783, 228426. https://doi.org/10.1016/j.tecto.2020.228426

Tables

Due to technical limitations, table 1,2,3 is only available as a download in the Supplemental Files section.

Figures

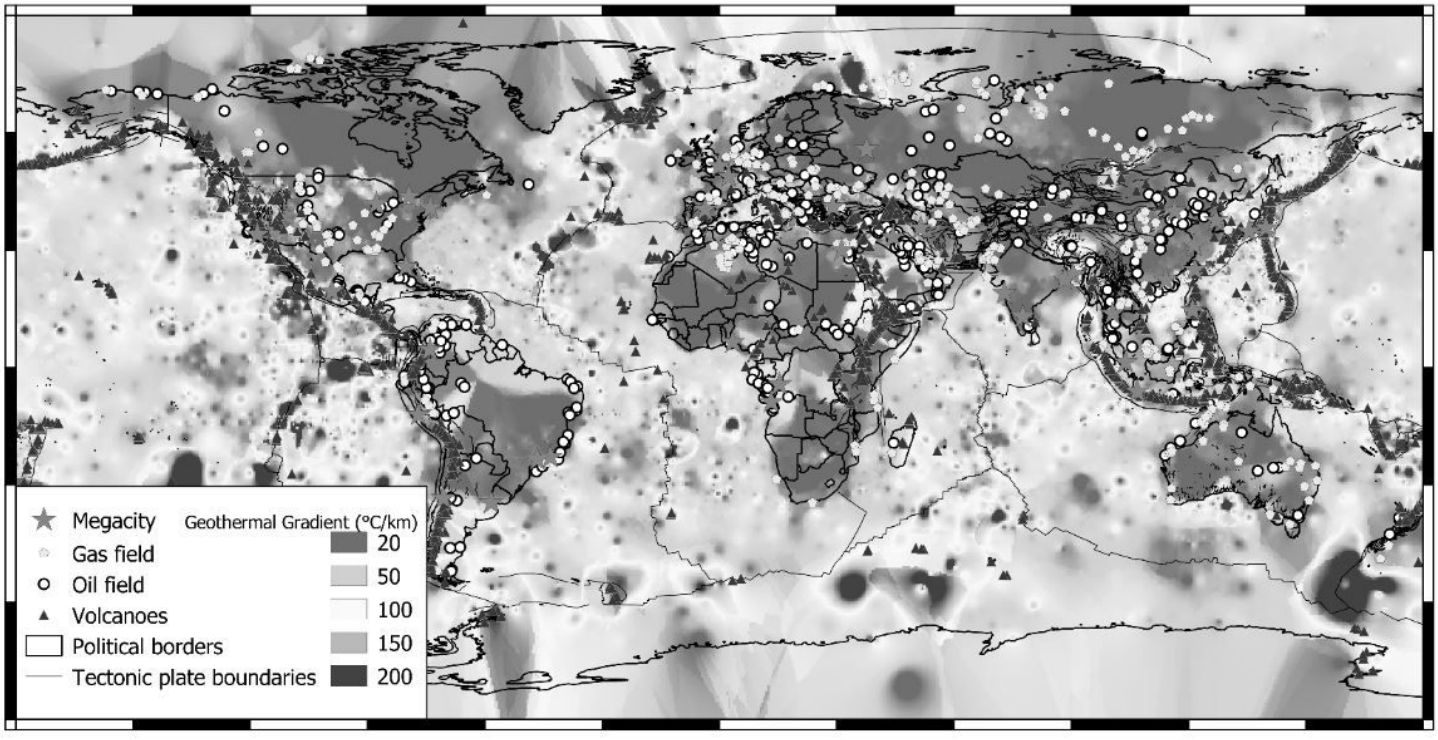

Figure 1

Worldwide distribution of geothermal gradient anomalies. Locations of volcanic belts and hydrocarbons occurrences have been combined with distribution of megacities. Note: The designations employed and the presentation of the material on this map do not imply the expression of any opinion whatsoever on

the part of Research Square concerning the legal status of any country, territory, city or area or of its authorities, or concerning the delimitation of its frontiers or boundaries. This map has been provided by the authors.

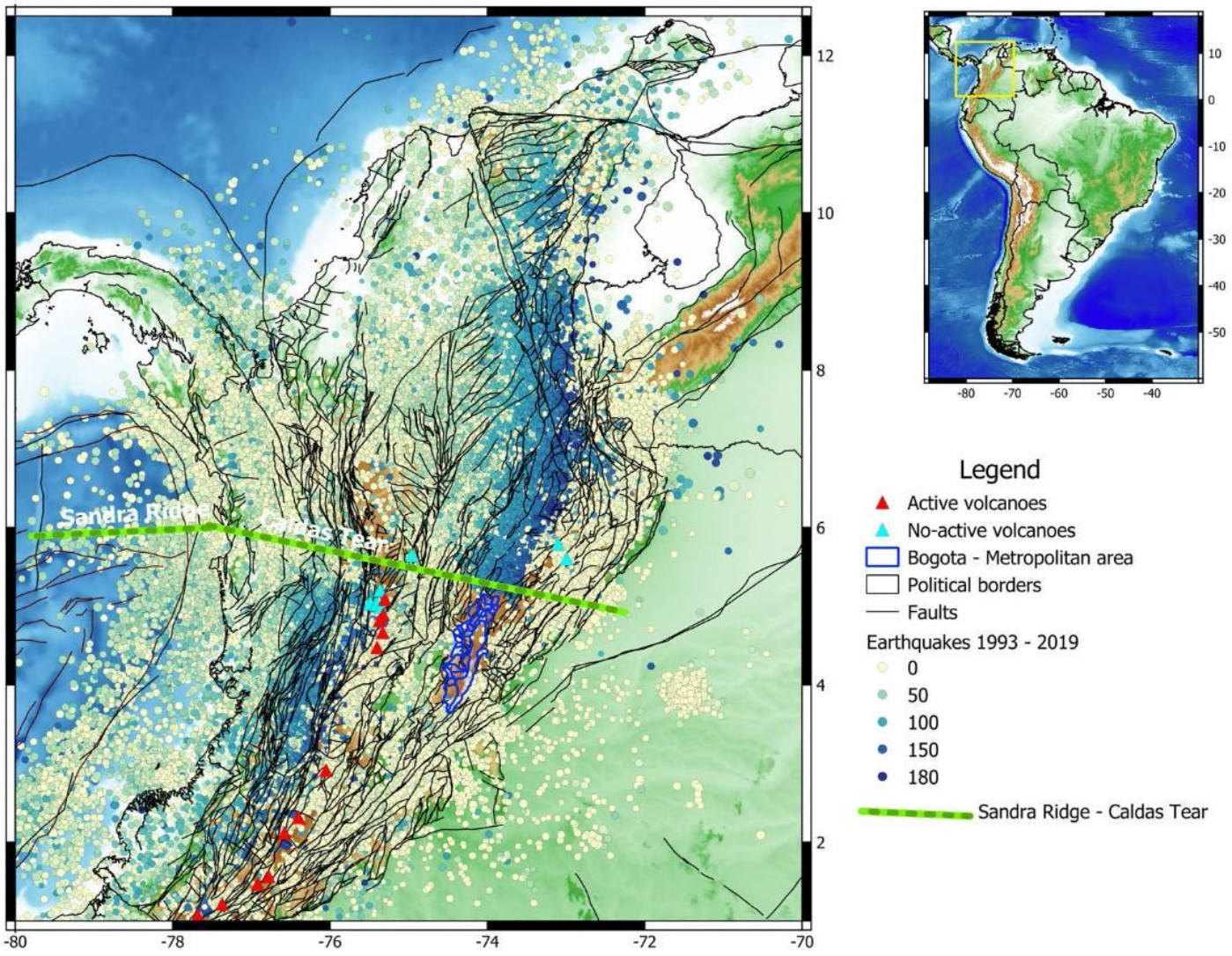

Figure 2

Upper: Distribution of seismicity in NW Colombia. Green-dashed line highlights the presence of a 240-km-long offset that displaces the subduction seismicity, which is called Caldas Tear. Lower: Geothermal gradient anomalies presented with spring-water occurrences (yellow circles), and O&G fields (purple diamonds). Black lines correspond to tectonic features. Red triangles are active volcanoes. Note: The designations employed and the presentation of the material on this map do not imply the expression of any opinion whatsoever on the part of Research Square concerning the legal status of any country, territory, city or area or of its authorities, or concerning the delimitation of its frontiers or boundaries. This map has been provided by the authors.

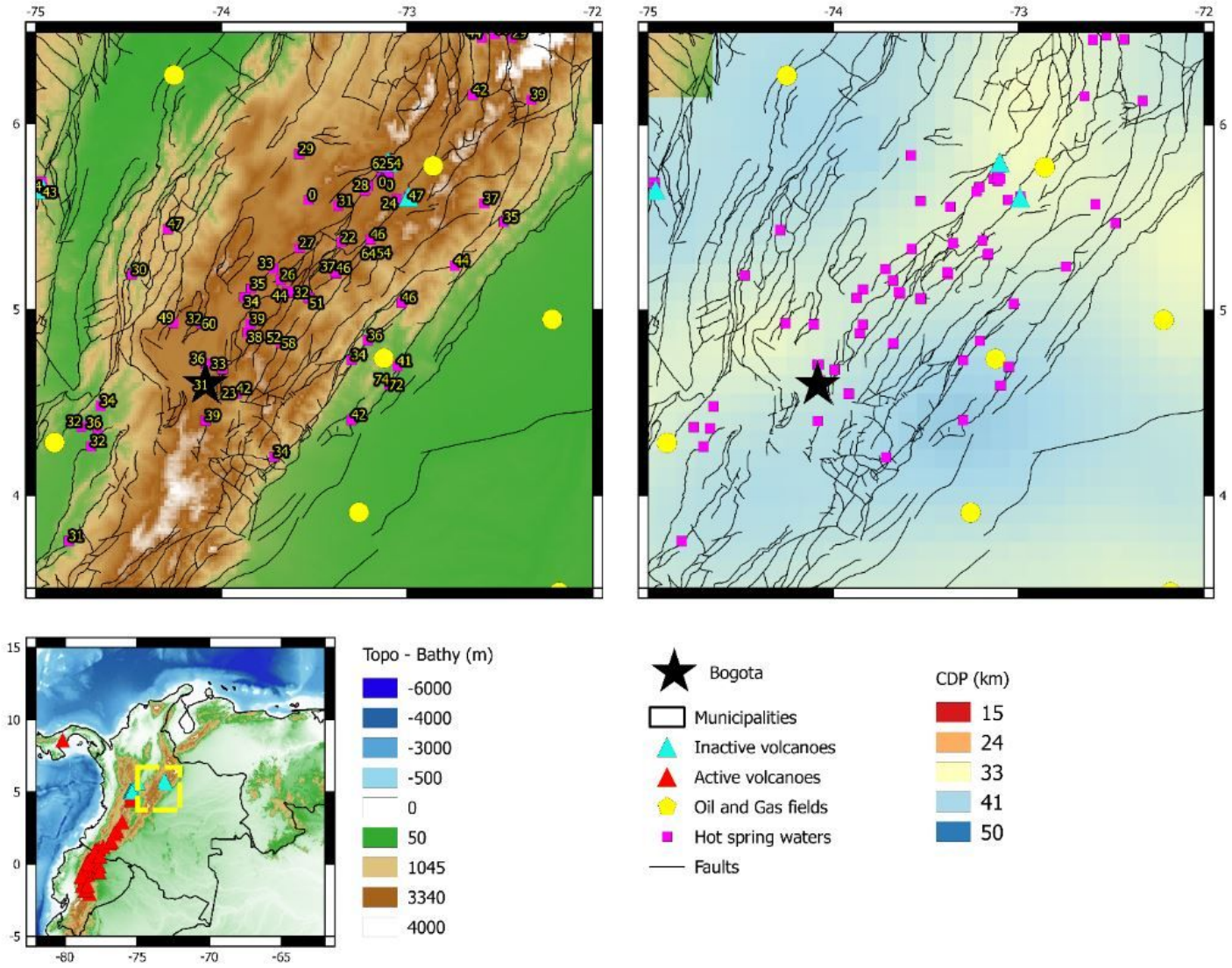

Figure 3

Upper-left map shows spring water occurrences (purple squares) with their average temperatures at north of Bogota. Upper-right map presents estimations of the Curie Point Depth (CPD) on same region (Li et al., 2017). Maps present faults (black lines), active volcanoes (red triangles), inactive volcanoes (cyan triangles), and O&G fields (yellow dots). Topography from Amante and Eakins (2009). Note: The designations employed and the presentation of the material on this map do not imply the expression of any opinion whatsoever on the part of Research Square concerning the legal status of any country, territory, city or area or of its authorities, or concerning the delimitation of its frontiers or boundaries. This map has been provided by the authors.

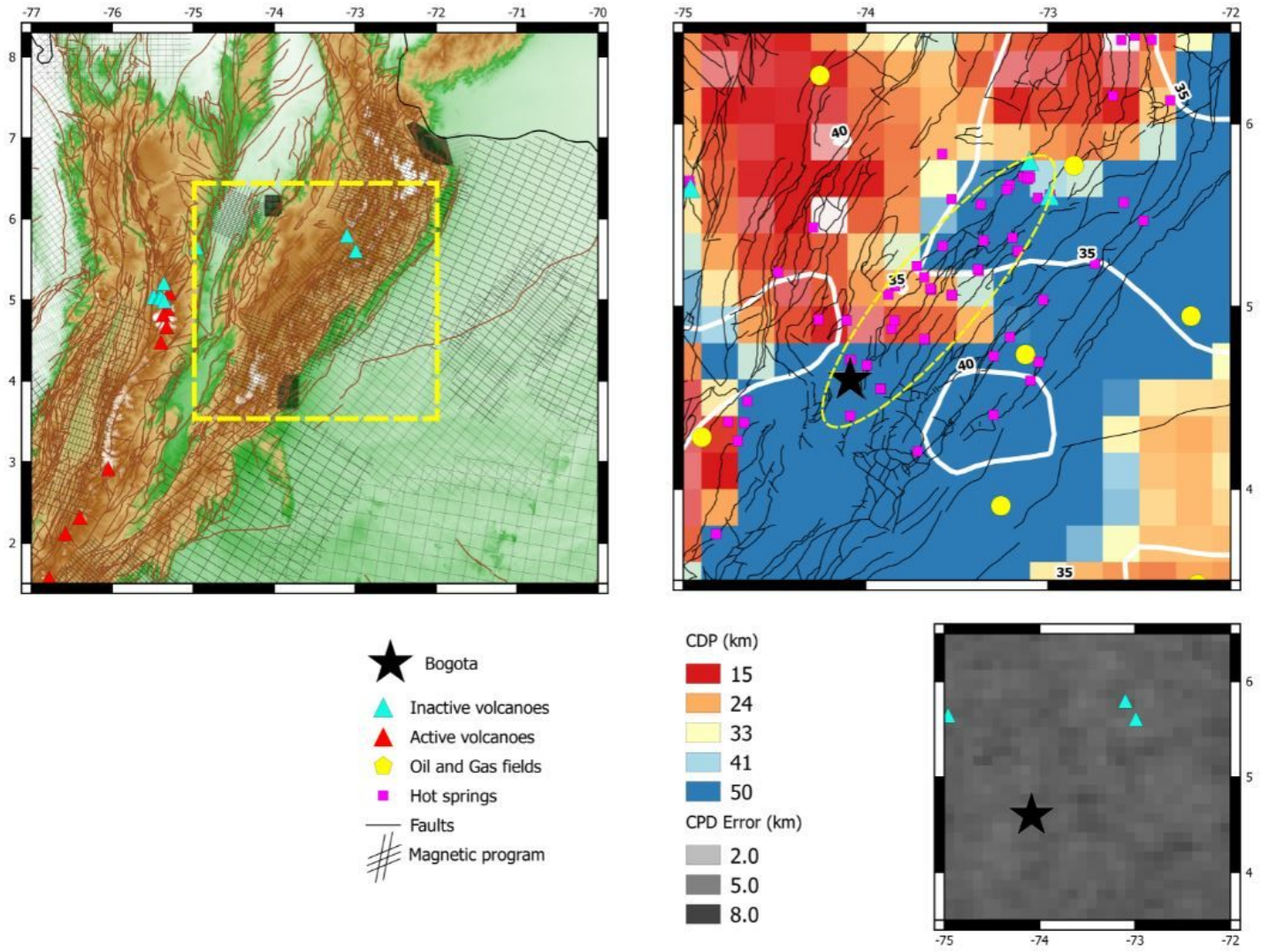

Figure 4

Upper-left map shows aeromagnetic programs flown on and near to the Eastern Cordillera, Colombia (black lines) and used to estimate the Curie Point Depth (CPD). Upper-right map presents estimations of the CPD in this work (coloured mosaic) and compared with the isodepths (white bold line) of CPD from Li et al. (2017). Maps present faults (black lines), active volcanoes (red triangles), inactive volcanoes (cyan triangles), hot springs (purple squares), and O&G fields (yellow dots). Yellow-dashed ellipse represents a hypothetical envelope that encompasses the main geothermal leads. Lower -right map corresponds to the error estimations of the CPD. Topography from Amante and Eakins (2009). Note: The designations employed and the presentation of the material on this map do not imply the expression of any opinion whatsoever on the part of Research Square concerning the legal status of any country, territory, city or area or of its authorities, or concerning the delimitation of its frontiers or boundaries. This map has been provided by the authors.

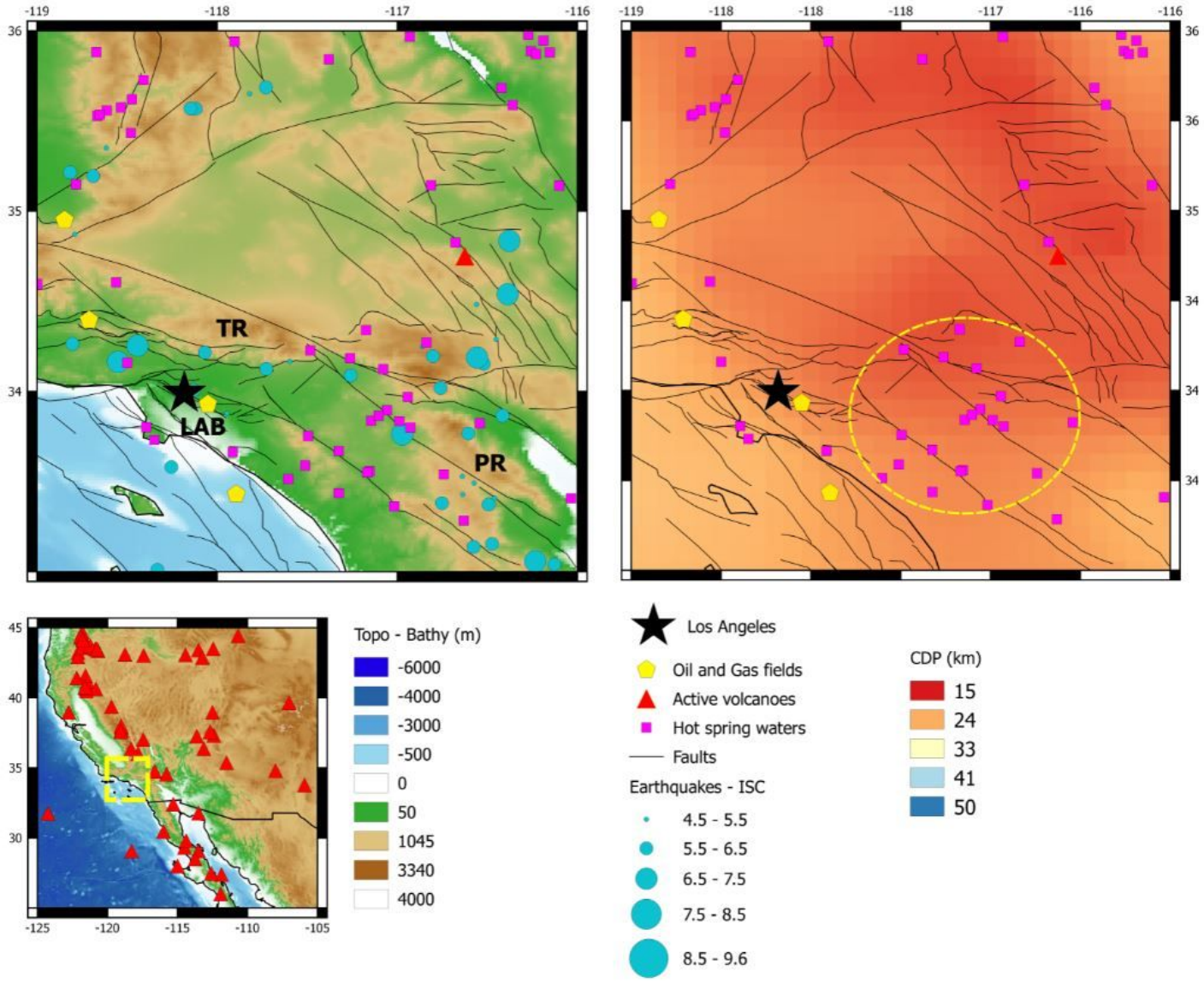

Figure 5

Upper-left map shows spring water occurrences (purple squares) near to Los Angeles (California). Upper-right map presents estimations of the Curie Point Depth (CPD) on same region (Li et al., 2017). Yellow-dashed ellipse represents a hypothetical envelope that encompasses the main geothermal leads. Maps present active volcanoes (red triangles), and O&G fields (yellow dots). Topography from Amante and Eakins (2009). Note: The designations employed and the presentation of the material on this map do not imply the expression of any opinion whatsoever on the part of Research Square concerning the legal status of any country, territory, city or area or of its authorities, or concerning the delimitation of its frontiers or boundaries. This map has been provided by the authors.

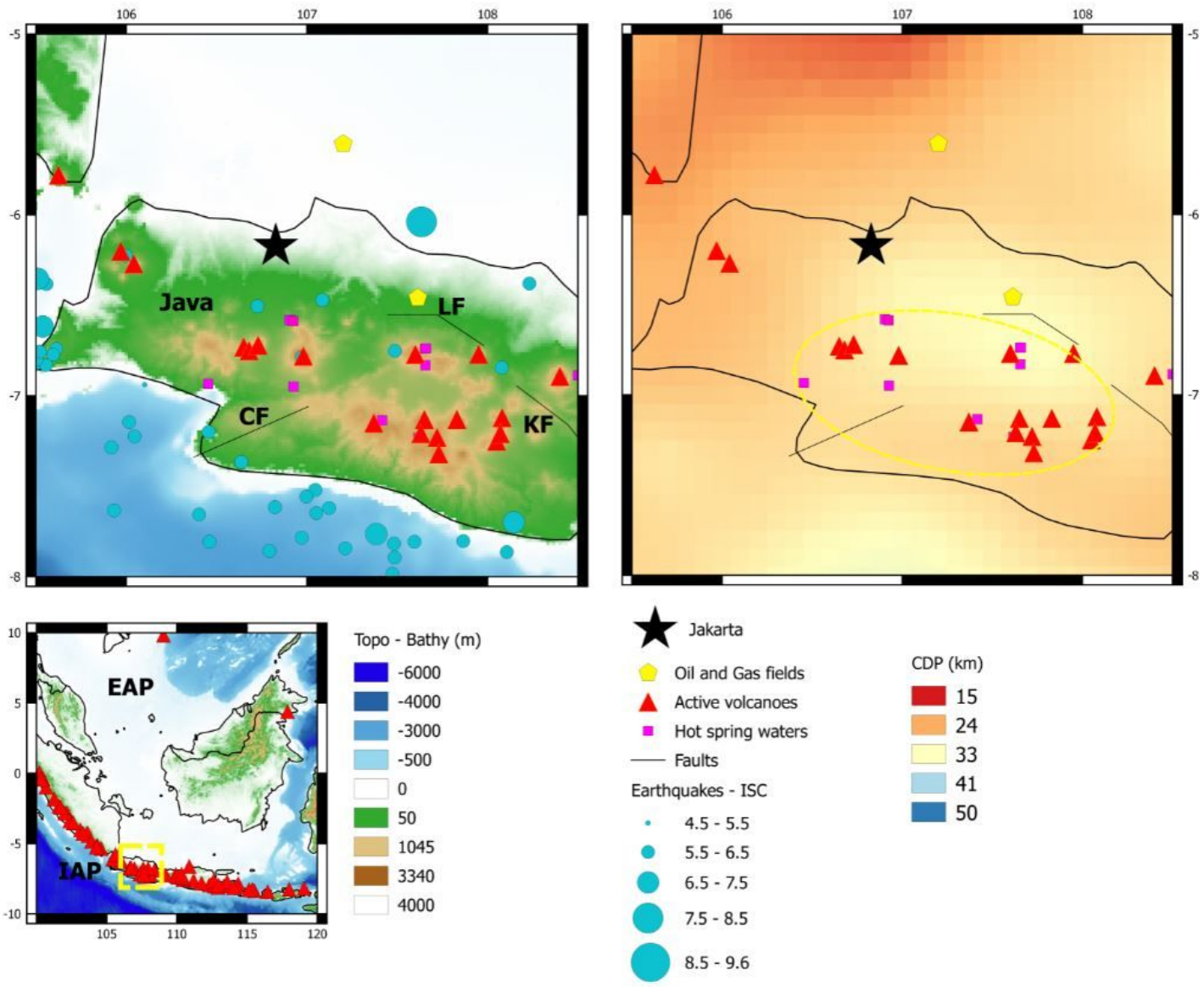

Figure 6

Upper-left map shows spring water occurrences (purple squares) near to Jakarta (Indonesia). Upper-right map presents estimations of the Curie Point Depth (CPD) on same region (Li et al., 2017). Yellow-dashed ellipse represents a hypothetical envelope that encompasses the main geothermal leads. Maps present active volcanoes (red triangles), and O&G fields (yellow dots). Topography from Amante and Eakins (2009). Note: The designations employed and the presentation of the material on this map do not imply the expression of any opinion whatsoever on the part of Research Square concerning the legal status of any country, territory, city or area or of its authorities, or concerning the delimitation of its frontiers or boundaries. This map has been provided by the authors.

Supplementary Files

This is a list of supplementary files associated with this preprint. Click to download.

- Table1.xlsx
- Table2.xlsx
- Table3.xlsx
- SupplementarymaterialHeatingCoolingNeedsMegacities.xlsx
- Annex.docx